

Ocean, land, and atmosphere (OLA): a simple climate emulator for net-zero emission scenarios^{*}

Aryan Eftekhari,[†] Pratyuksh Bansal,[‡] Doris Folini,[§] Felix Kübler,[¶]
Aleksandra Malova,^{||} Simon Scheidegger,^{**} Olaf Schenk^{††}

September 18, 2023

Abstract

We extend DICE-2016 with another time scale
Wish list:

- Extreme econ cases to confront with different carbon cycles

Keywords: climate change, social cost of carbon, carbon taxes, environmental policy, deep learning, integrated assessment models, DICE-2016

JEL classification: C61, E27, Q5, Q51, Q54, Q58

^{*}We thank ..., as well as seminar participants at the University of Lausanne and the University of Zurich for very useful conversations and comments. This work was supported by the Swiss National Science Foundation (SNF), under project ID “Can Economic Policy Mitigate Climate-Change?”, and for research support. Simon Scheidegger gratefully acknowledges support from the MIT Sloan School of Management.

[†]TBA, UNI; Email: bla.ch.

[‡]Institute of Computing, Università della Svizzera italiana; Email: pratyuksh.bansal@sam.math.ethz.ch.

[§]Institute for Atmospheric and Climate Science, ETHZ; Email: doris.folini@env.ethz.ch.

[¶]Department for Banking and Finance, University of Zürich; Swiss Finance Institute (SFI); Email: felix.kuebler@bf.uzh.ch.

^{||}Department of Economics, University of Lausanne; Email: aleksandra.malova@unil.ch.

^{**}Department of Economics, University of Lausanne; Enterprise for Society (E4S); Email: simon.scheidegger@unil.ch

^{††}Institute of Computing, Università della Svizzera italiana; Email: olaf.schenk@usi.ch.

Summary

1	Introduction	3
2	Climate Emulator	5
2.1	Carbon-Cycle	5
2.2	Fitting Procedure	6
2.2.1	Mean Parameters	7
2.2.2	Extrema Parameters	8
2.3	Calibration	9
3	Simulations	11
3.1	Atmospheric Perturbation Tests	11
3.1.1	Pulse	12
3.1.2	macdougall	13
3.2	Representative Concentration Pathway	14
A	Climate Emulator	17
B	Temperature Model	22

1 Introduction

Suggested storyline:

- 1 paragraph blabla
- motivations of current paper: point out of current DICE (e.g., RCP)
- on an abstract level: 1 dynamic timescale missing.
- on a concrete level. We cannot resolve e.g. RCP2.6
- What are the economic implications: aggressive mitigation cannot be handled, etc...
- contribution from our side: go from 3 to 4 or 5 reservoirs.
- show how to calibrate it. Extend also test set by more tests (CDICE) to pin down the additional degrees of freedom.
- Contribution to climate science as stand-alone (preview of results): with this simple model(s), we show that we can correctly capture a),b),c), which contradicts the present opinion in the literature.
- from an econ applications point of view,

Climate modeling in the context of economic modeling consists, in essence, of translating carbon emissions generated by economic activity into atmospheric CO₂ concentrations and on into a change in global mean temperature. Associated climate emulators (CEs) need to be computationally cheap, to free resources for the modeling of any none-climate aspects, yet 'fit for purpose'¹. The pivotal role of equilibrium climate sensitivity (ECS) when calculating the temperature change arising from an increase in atmospheric CO₂ has long been recognized. A plausible reason why ECS has attracted so much attention from the economic community may be the uncertainty of ECS from a climate science point of view. Best estimates for ECS still range from roughly 2 to 4 degree Celsius, thus cannot be simply ignored in an economic context. Comparatively less attention is paid to uncertainties associated with the carbon-cycle, the second pillar of any climate model used in an economic context. Associated models vary in their level of complexity, ranging from simple impulse response function or two layer box models to more comprehensive models designed, for example, to account for hemispheric and depth dependent aspects of the oceans and to capture aspects of the land biosphere. The performance of one such model, a three-reservoir carbon-cycle model as used in the seminal DICE model, was assessed in some detail by Folini et al. (2022) from a climate science point of view and with regard to the impact of the carbon-cycle on economic aspects. It was demonstrated that i) a correct calibration of the carbon-cycle with respect to climate science bench marks is crucial and that ii) varying model calibration within bounds justified by climate science has a relevant impacts on economics, about half as big as from varying ECS (see Figure 12a in Folini et al. (2022)). The paper further stressed the relevance of the three-box carbon-cycle model featuring two response time scales, a fast and a slow one, in order to properly translate carbon emissions into atmospheric CO₂ concentrations.

The present paper is a follow-up on Folini et al. (2022) in that it addresses the question of whether adding more carbon reservoirs has a relevant effect on the performance of the CE with regard to climate science and economics. We examine models consisting of three, four, or five carbon reservoirs that represent the atmosphere, the ocean, and possibly the biosphere on land. Addition of a land biosphere reservoir also paves the way to study climate mitigation scenarios explicitly involving the land biosphere for carbon capture and storage. The later question is of relevance in view of the Paris agreement and associated climate targets, like the 1.5 degree target. Climate science claims that reaching these goals implies a rapid decline in emission and even negative emissions later in this

¹See Folini et al. (2022) for a more detailed discussion of what is meant by 'fit for purpose'.

century. The question arises whether simple carbon-cycle models as studied here are fit to purpose in view of such scenarios.

Mitigation scenarios distinguish themselves from business as usual scenarios in that carbon emissions decrease or even become negative (carbon sequestration) instead of steadily growing. From a carbon-cycle point of view this implies that partial pressure differences between notably the atmosphere and the ocean become smaller with time, as carbon emissions to the atmosphere diminish. With the difference in CO₂ partial pressure between atmosphere and ocean diminishing, the uptake efficiency of the ocean decreases. Under extreme scenarios, the ocean may even turn from a CO₂ sink to a CO₂ source. Modeling of such behavior, of such re-distribution of carbon among reservoirs, necessitates that the entity of emitted carbon over time is still present in the model. This is the case for carbon-cycle box models, but not necessarily for impulse response function models. We quantify the capability of the simple box models at the heart of this study to successfully emulate this behavior, making the models suitable to study the connection between economy, strong mitigation scenarios, and climate.

We start from the functional form of the carbon-cycle as used in the widely used DICE-2016 model, a three-box model with one box for the atmosphere and two boxes for the ocean, one for the upper-ocean one for the deep-ocean. We add more reservoirs to the carbon-cycle model and follow the strategy outlined in Folini et al. (2022) to calibrate and bench mark the model. We note already here that additional bench marks specifically tailored to negative emissions or the land-biosphere reservoir do not form part of this study and are the topic of future work. Finally, we apply the newly calibrated carbon-cycle models to examine optimal abatement policies, focusing on whether the additional carbon-reservoirs make any difference in this respect. The paper is organized as follows.

Things to stay before section 2

- Pre-industrial is assume do 1765
- Carbon REservoires at pre-industrial times are based on https://www.ipcc.ch/site/assets/uploads/2018/02/WG1AR5_Chapter06_FINAL.pdf
- Stability: Reduces variability in parameter estimates for different benchmark.
- short-time dynamics Salient
- Short-Term absorption discrepancy.

2 Climate Emulator

In this section, we will present our proposed methodology for a climate emulator, namely the carbon-cycle model, estimation procedure and calibration. We propose two carbon-cycle model configurations, which use serial and parallel reservoir configurations. The models we considered include three reservoir classes: atmosphere (A), ocean (O), and land-biosphere (L). In the serial model, labeled as 3SR, the carbon cycle is modeled as three sequentially connected carbon reservoirs, with the atmosphere connected to the upper ocean O_1 , and the ocean connected to the deep ocean O_2 . The parallel model labels 4PR, introduces the land-biosphere, where carbon from the atmosphere is divided into two parallel streams: land-biosphere and ocean. The 4PR model is an extension of 3SR model by adding a single land biosphere reservoir (L); see, Figure 1 for visualization.

[more text]

[more text]

2.1 Carbon-Cycle

Let $\mathbf{m}^t \in \mathbb{R}^n$ be the amounts of carbon in p distinct reservoirs at discrete time steps $t = 1, 2, \dots, T$. The carbon-cycle model can be characterized by the time-invariant operator $\mathbf{A} \in \mathbb{R}^{n \times n}$, which determines the rate of carbon mass exchange between these reservoirs. Accounting for emissions, denoted by $\mathbf{e}^t \in \mathbb{R}^n$, we describe the carbon-cycle using a first-order system of difference equations

$$\mathbf{m}^t - \mathbf{m}^{t-1} = \mathbf{A}\mathbf{m}^t + \mathbf{e}^t, \quad (1)$$

where, h is the time-step size, and where \mathbf{m}^0 is the *initial condition*, which is known. Throughout this paper we assume $h = 1$. The operator \mathbf{A} possess real eigenvalues $-1 < \lambda_i(\mathbf{A}) \leq 0$ for all i . For i and j , there exists a carbon transfer path between the reservoirs if $\mathbf{A}_{ij} \neq 0$, and there is no carbon transfer path if $\mathbf{A}_{ij} = 0$. Furthermore, \mathbf{A} is restricted to satisfy both the equilibrium condition and the system mass conservation. The equilibrium conditions of the carbon-cycle are defined as

$$\mathbf{A}\tilde{\mathbf{m}} = \mathbf{0}, \quad (2)$$

where $\tilde{\mathbf{m}}$ denotes the equilibrium carbon masses, which is proportional to the eigenvector associated with the zero eigenvalue of \mathbf{A} . The principle of mass conservation is upheld by ensuring that

$$\mathbf{1}^\top (\mathbf{m}^t - \mathbf{m}^{t-1}) = \mathbf{e}^t \forall t \iff \mathbf{1}^\top \mathbf{A} = \mathbf{0}. \quad (3)$$

We define the *dynamic timescales* of the operator as $\tau_i = 1/|\lambda_i|$, excluding the zero eigenvalue, which corresponds to the infinite timescale associated with the equilibrium condition. Consequently, the potential dynamic timescales for the linear carbon-cycle model are $\tau_i \in (1, \infty)$.

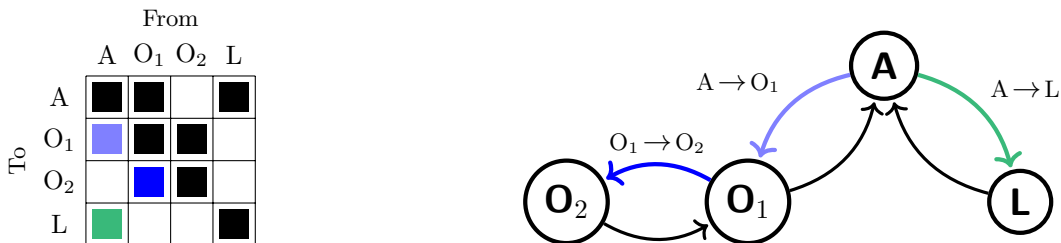


Figure 1: The operator \mathbf{A} is visualized (left) for the 4PR model, which includes atmosphere (A), two ocean reservoirs (O_1 and O_2), and a land reservoirs (L). A graphically representation of the connectivity of the reservoirs (right) is shown with the unknown carbon mass transfer rates denoted, for example, $O_1 \rightarrow O_2$ corresponds to the entry $\mathbf{A}_{3,2}$. The 3SR model is a can all be considered as subsets of the more complex 4PR model configuration. \mathbf{A} is symmetric in its nonzero pattern, but not in its values.

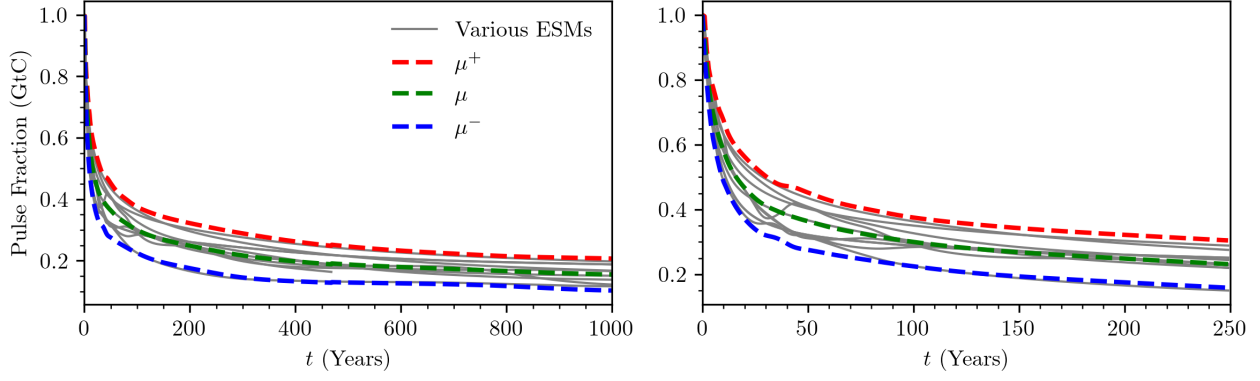


Figure 2: The decay of a 100 GtC pulse of emissions in the pre-industrial atmosphere (1765) was analyzed using various Earth System Models of differing complexities. This data is based on a series of controlled simulations conducted by Joos et al. (2013). The multimodal mean of the simulations, denoted by μ , along with the two standard deviations above and below μ -benchmark, are represented by μ^+ and μ^- , respectively.

Denote the nonzero strictly lower-triangular indices of \mathbf{A} as $\mathcal{I} := \{(i, j) : \mathbf{A}_{ij} \neq 0, i > j\}$. For all model configurations outlined, the closed-form solutions for the upper triangular values of the operator satisfying both (2) and (3) is

$$\mathbf{A}_{ji} = \mathbf{A}_{ij} \frac{\tilde{\mathbf{m}}_j}{\tilde{\mathbf{m}}_i} \quad \forall (i, j) \in \mathcal{I}, \text{ and } \mathbf{A}_{ii} = - \sum_{j=1, j \neq i}^p \mathbf{A}_{ij}. \quad (4)$$

The necessary admissible parameters required to define the operator include the strictly lower triangular nonzero values $\mathbf{a} := \{\mathbf{A}_{ij} : (i, j) \in \mathcal{I}\}$ and the equilibrium masses $\tilde{\mathbf{m}}$, for which the parameterized operator, denoted as $\mathbf{A}[\mathbf{a}, \tilde{\mathbf{m}}]$ has eigenvalues satisfying $-1 < \lambda_i(\mathbf{A}[\mathbf{a}, \tilde{\mathbf{m}}]) \leq 0$. For a predefined sequence of emissions $\mathbf{E} := (\mathbf{e}^1, \mathbf{e}^2, \dots, \mathbf{e}^T)$ of length T the carbon-cycle simulation denoted as

$$\mathbf{M}[\mathbf{a}, \tilde{\mathbf{m}}] := (\mathbf{m}^1, \mathbf{m}^2, \dots, \mathbf{m}^T), \quad (5)$$

where \mathbf{m}^t is defined as per (1). We utilize acronyms depicted in Figure 1 to refer to specific reservoirs; for instance, $\mathbf{M}[\mathbf{a}, \tilde{\mathbf{m}}]_{\text{O}_2}^t$ (or simply $\mathbf{m}_{\text{O}_2}^t$ when \mathbf{a} and \mathbf{m} do not need to be emphasized) represents the content of the O_2 or deep-ocean reservoir at time t . Throughout this section, our simulations are exclusively use atmospheric emissions, meaning \mathbf{e}_A^t is nonzero only when emissions are present at time t , while all other entries are zero.

2.2 Fitting Procedure

The proposed linear carbon-cycle is a simplified approximation of a considerably more complex system; our goal here to fit the model parameters for the 3SR and 4PR model configuration, such that we capture the salient dynamics of the carbon-cycle. The proposed parameter fitting procedure aims to capture the pulse decay dynamics using a two-step process: first, we optimize the model parameters to emulate mean atmospheric pulse decay trajectory of a selected benchmarks; second, we present an approach to scale the fitted model to capture the extrema benchmarks of various benchmarks. The simulation benchmarks introduced by Joos et al. (2013), and depicted in Figure 1, are use for the parameter fitting procedure. The benchmarks represent the atmospheric CO_2 decay trajectories of a 100 GtC pulse in various Earth System Models conducted in pre-industrial conditions in which the carbon-cycle is assumed to be at equilibrium.²

²See https://climatehomes.unibe.ch/~joos/IRF_Intercomparison/results.html for further details.

2.2.1 Mean Parameters

We fit the operator parameters \mathbf{a} and $\tilde{\mathbf{m}}$ to best emulate the atmospheric CO2 masses after a 100 GtC pulse. The benchmark used in the fitting procedure is the multimodal mean of the various decay trajectories, which is referred to as the μ -benchmark; see, Figure 1 for visualization. Specifically, we aim to minimize the discrepancy between the simulated atmospheric CO2 masses and those of the μ -benchmark, while simultaneously imposing penalties on solutions that fail to align with observed carbon-cycle attributes. These attributes are encoded via penalty functions q_1 , q_2 and q_3 , which related to (i) dynamic time-scales, (ii) variability in equilibrium masses, and (iii) reservoir absorption ratios, respectively. We will discuss the penalty functions in detail the paragraphs to follow.

Let $\mathbf{y}^\mu \in \mathbb{R}^T$ denote the atmospheric decay trajectory for the μ -benchmark for T years after the introduction of the 100 GtC pulse. The fit error which is measured solely based on the deviation between the emulated atmospheric masses and the μ -benchmark, is defined as

$$\mathcal{L}(\mathbf{a}^\mu, \tilde{\mathbf{m}}^\mu) := \frac{1}{T} \left\| \mathbf{M}[\mathbf{a}, \tilde{\mathbf{m}}]_{\mathbf{A}} - \mathbf{y}^\mu \right\|_2. \quad (6)$$

Note that the masses of other reservoirs are controlled through the penalty terms. Given the non-negative tuning coefficients ρ_1 , ρ_2 , and ρ_3 , each which correspond to the respective penalty functions, the μ -benchmark fitted parameters are

$$\left\{ \mathbf{a}^\mu, \tilde{\mathbf{m}}^\mu \right\} = \underset{\{\mathbf{a}, \tilde{\mathbf{m}}\}}{\operatorname{argmin}} \left\{ \mathcal{L}(\mathbf{a}^\mu, \tilde{\mathbf{m}}^\mu) + \rho_1 q_1(\mathbf{a}, \tilde{\mathbf{m}}) + \rho_2 q_2(\tilde{\mathbf{m}}) + \rho_3 q_3(\mathbf{a}, \tilde{\mathbf{m}}) \right\}. \quad (7)$$

Typically, we aim to minimize (7) so that we can accurately emulate relatively short time-frames; that is to say, for T is not so large. In our tests we use $T = 250$ aligning with the time scales associated with the carbon exchange between the atmosphere and the Earth's surface, which span years to centuries.

Dynamic Timescales: In addition to the carbon exchange between the atmosphere and the Earth's surface, we also take into account the long-term carbon cycles in deep soils and the deep ocean. These cycles occur over time frames ranging from centuries to millennia. To better mimic these carbon-cycle processes—especially those extending over longer dynamical time scales—the objective function (7) incorporates the penalty function

$$q_1(\mathbf{a}, \tilde{\mathbf{m}}) := -\frac{1}{n} \operatorname{tr}(\mathbf{A}[\mathbf{a}, \tilde{\mathbf{m}}]) = -\frac{1}{n} \sum_{i=1}^n \lambda_i(\mathbf{A}[\mathbf{a}, \tilde{\mathbf{m}}]). \quad (8)$$

This modification effectively biases the optimization program to favor operators $\mathbf{A}[\mathbf{a}, \tilde{\mathbf{m}}]$ characterized by smaller average eigenvalues, or equivalently, by larger average time scales. It is important to note that for all admissible parameters \mathbf{a} and $\tilde{\mathbf{m}}$, (8) is strictly-positive.

Equilibrium Mass Variability: The optimization problem in (7) is not convex; this is clearly seen in (4), were only the ratios of $\tilde{\mathbf{m}}$ are relevant; this implies that scalar multiple of $\tilde{\mathbf{m}}$ is equivalent. As a result we can expect a high-degree of variability in the fitted parameter \mathbf{a} and $\tilde{\mathbf{m}}$. To address this issue, we induce a bias in the objective to ensure that $\tilde{\mathbf{m}}$ aligns with existing estimates of Earth's pre-industrial carbon reservoirs masses. Let $\tilde{\mathbf{m}}^*$ denote the estimated reservoir equilibrium masses. We penalize the relative difference of $\tilde{\mathbf{m}}$ with respect to $\tilde{\mathbf{m}}^*$ using the penalty function

$$q_2(\tilde{\mathbf{m}}) := \frac{1}{n} \left\| (\tilde{\mathbf{m}} - \tilde{\mathbf{m}}^*) \oslash \tilde{\mathbf{m}}^* \right\|_2. \quad (9)$$

where \oslash denote the elements-wise division. In our tests, $\tilde{\mathbf{m}}^*$ is defined based one pre-industrial estimates outlined in Ciais et al. (2014) where the reservoir equilibrium masses for the atmosphere, upper ocean, lower ocean, and land biosphere are 589, 900, 37 100, and 550 GtC, respectively.

Reservoir Absorption Ratios: Cumulative fluxes of carbon from the atmosphere to the ocean and land biosphere reservoirs significantly influence the overall response characteristics of the emulator. For instance, in the context of the 100 GtC pulse, it is plausible that the 4PR configuration could achieve a good fit for the atmospheric decay trajectory while maintaining minimal cumulative flux in the reservoir associated with land biosphere—essentially mimicking the behavior of the 3SR model which lacks a land biosphere reservoir (see, e.g., Section ?? for further details). To ensure that the model mirrors the observed dynamics in the more complex Earth System Model (ESM), we enforce the ratios of cumulative ocean and land biosphere fluxes, denoted as η , at specific time period following the emission at t_e . To approximate the cumulative ocean and land-biosphere flux ratio as η at time t_e , deviations from this value is penalized using the penalty function

$$q_3(\mathbf{a}, \tilde{\mathbf{m}}) := \left\| \frac{\mathbf{M}[\mathbf{a}, \tilde{\mathbf{m}}]_{\text{O}}^{t_e}}{\mathbf{M}[\mathbf{a}, \tilde{\mathbf{m}}]_{\text{L}}^{t_e}} - \eta \right\|_2, \quad (10)$$

where $\mathbf{M}[\mathbf{a}, \tilde{\mathbf{m}}]_{\text{O}}^{t_e}$ is the total mass of all ocean reservoirs (and similarly, the superscript L denotes all land biosphere reservoirs). We adopt the findings of Joos et al. (2013), whose experiments show that an equal 30 GtC distribution between ocean and land-biosphere reservoirs is achieved, corresponding to $\eta = 1$, at $t_e = 20$ years after a 100 GtC atmospheric pulse. These are average values, for which any individual ESM may have differing values.

2.2.2 Extrema Parameters

As illustrated in Figure 2, various ESMs demonstrate different rates of 100 GtC pulse decay trajectories. Here we aim to capture the extrema of these trajectories across different ESMs (see, e.g., Figure 2). Similar to the mean fitting procedure outlined in the preceding section, these dynamics are not intrinsically linked to any particular ESM; rather, they define the plausible upper and lower limits for atmospheric carbon content during such a pulse event. The proposed approach aims augmenting the fitted operator outlined in the previous section to represent two standard deviations above and below the μ -benchmark, denoted as μ^+ and μ^- -benchmark, respectively.

Let $c^{\mu^-}, c^{\mu^+} \in \mathbb{R}^+$ be positive coefficients, corresponding to the μ^+ and μ^- -benchmark decay trajectories, respectively. For $\mathbf{A}^\mu := \mathbf{A}[\mathbf{a}^\mu, \tilde{\mathbf{m}}^\mu]$, we represent the respective extrema operators as $\mathbf{A}^{\mu^+} := c^{\mu^+} \cdot \mathbf{A}^\mu$ and $\mathbf{A}^{\mu^-} := c^{\mu^-} \cdot \mathbf{A}^\mu$. Given the pulse decay trajectories $\mathbf{y}^{\mu^+}, \mathbf{y}^{\mu^-} \in \mathbb{R}^T$, with

$$c^{\mu^+} = \underset{c}{\operatorname{argmin}} \left\{ \frac{1}{T} \left\| \mathbf{M}[c \cdot \mathbf{a}^\mu, \tilde{\mathbf{m}}^\mu]_{\text{A}} - \mathbf{y}^{\mu^+} \right\|_2 \right\}, \text{ and } c^{\mu^-} = \underset{c}{\operatorname{argmin}} \left\{ \frac{1}{T} \left\| \mathbf{M}[c \cdot \mathbf{a}^\mu, \tilde{\mathbf{m}}^\mu]_{\text{A}} - \mathbf{y}^{\mu^-} \right\|_2 \right\}. \quad (11)$$

In our test, we keep T the same value as described in (7). Notice that \mathbf{A}^{μ^+} and \mathbf{A}^{μ^-} are essentially \mathbf{A}^μ , but with all its eigenvalues scaled by the factors c^{μ^+} and c^{μ^-} , respectively. By adjusting the eigenvalues, we shift the range of dynamical timescales either upward or downward by a fixed proportion.

The solution of (11) will be such that $c^{\mu^+} < 1 < c^{\mu^-}$. Owing to the linearity of the proposed carbon-cycle model, we are able to formulate a parameterized weighted operator that spans the full range of possible operators. Given $\alpha \in [-1, 1]$, the weighted operator is

$$\mathbf{A}^\alpha := \begin{cases} (1 - \alpha)\mathbf{A}^\mu + \alpha\mathbf{A}^{\mu^+} & \text{if } \alpha > 0 \\ (1 + \alpha)\mathbf{A}^\mu - \alpha\mathbf{A}^{\mu^-} & \text{otherwise,} \end{cases} \quad (12)$$

where $\alpha = 0$ emulates the mean atmospheric carbon content across various ESMs, and $\alpha = 1$ or -1 we emulate ESMs with higher or lower atmospheric carbon content (slow or fast carbon absorption out of the atmosphere), respectively. It is important to note that the weighted operator shares the same equilibrium condition, with $\mathbf{A}^\alpha \tilde{\mathbf{m}}^\mu = \mathbf{0}$ for all values of α .

2.3 Calibration

Here we outline the calibration procedure for the tuning coefficients and the resulting fitted described in Section 2.2. In all tests conducted, we fix $\tilde{\mathbf{m}}_A = 586$, which corresponds to the preindustrial atmospheric equilibrium condition [Ciais et al. \(2014\)](#).

We first focus on the tuning coefficients ρ_2 and ρ_3 related to equilibrium mass variability and reservoir absorption ratios, respectively. In general we want to use smaller tuning coefficients to avoid suboptimal outcomes where penalty functions outweigh model fit (6). Based on our experimental results, for both 3SR and 4PR model configuration, we fix the tuning coefficients $\rho_2 = \rho_3 = 10^{-4}$ which minimizes the impact on the fit error while sufficiently large to induce the desired change in the equilibrium mass and reservoir absorption ratios (see Section 2.2.1 for details on the q_1 and q_2 penalty functions). Note that for the 3SR configuration, q_3 has no influence as the model lacks a land-biosphere component. In Figure A.1 we show the effects of the penalty functions, or equivalent the tuning coefficients ρ_2 and ρ_3 on the emulated pulse decay. Setting either ρ_2 or ρ_3 to 10^{-4} (while keeping $\rho_1 = 0$) results in minimal changes to the overall dynamics of the 3SR model, but leads to a significant change in the cumulative flux absorption across the reservoirs in the 4PR model. As the 3SR model has fewer degrees of freedom than the 4PR configuration it appears that the convergence of (7) is primarily driven by reducing the pulse decay fit error rather than optimizing other penalty terms. In contrast, the 4PR model permits equally low pulse decay fit errors, but with a varying range of carbon absorption dynamics—highlighting the importance of penalty methods for constraining the

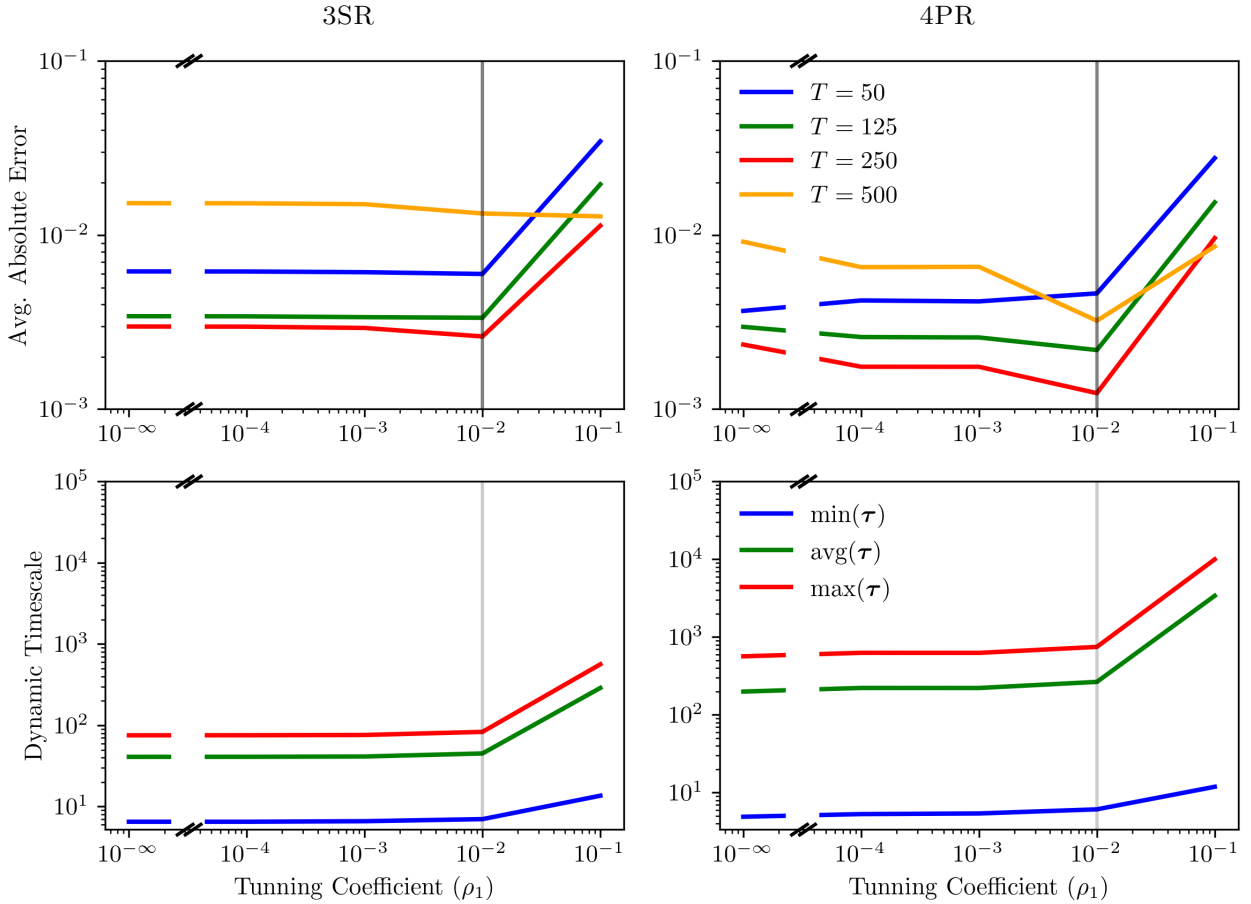


Figure 3: The average absolute error and dynamic timescales τ for the 3SR (left column) and 4PR (right column) model configuration for varying values of ρ_1 at fixed value of $\rho_2 = \rho_3 = 10^{-4}$. The displayed error is calculated as the absolute difference between the emulator simulation and the μ -benchmark, averaged over a timespan of T years following a 100 GtC carbon pulse. The black vertical line is the selected value $\rho_1 = 10^{-2}$.

	FITTED PARAMETERS VALUES											
	$\mathbf{a}_{\text{A} \rightarrow \text{O}_1}^\mu$	$\mathbf{a}_{\text{O}_1 \rightarrow \text{O}_2}^\mu$	$\mathbf{a}_{\text{A} \rightarrow \text{L}}^\mu$	$\tilde{\mathbf{m}}_{\text{A}}^\mu$	$\tilde{\mathbf{m}}_{\text{O}_1}^\mu$	$\tilde{\mathbf{m}}_{\text{O}_2}^\mu$	$\tilde{\mathbf{m}}_{\text{L}}^\mu$	\mathbf{c}^{μ^+}	\mathbf{c}^{μ^-}	$\mathbf{m}_{\text{O}}^{t_e}/\mathbf{m}_{\text{L}}^{t_e}$	τ	
<i>Lower</i>	10^{-6}	10^{-6}	10^{-6}	589	10^{-6}	10^{-6}	10^{-6}	10^{-6}	1			
3SR	0.077	0.011	-	589	752	1,289	-	0.475	2.456	-	7/83	
4PR	0.021	0.003	0.061	589	1,078	37,255	387	0.470	2.407	0.71	6/42/748	
<i>Upper</i>	0.3	0.3	0.3	589	1,800	74,200	1,100	1	5			

Table 1: The table shows the fitted parameter values, ratio of ocean and land-biosphere pulse absorption ($\mathbf{m}_O^{t_e}/\mathbf{m}_L^{t_e}$), and dynamic timescales (τ), based on tuning coefficients ρ_1 , ρ_2 , and ρ_3 , with respective values 10^{-2} , 10^{-4} , and 0.0 for the 3SR model, and 10^{-2} , 10^{-4} , and 10^{-4} for the 4PR model. The ratio of ocean and land-biosphere pulse absorption is measured at $t_e = 20$ and $\tilde{\mathbf{m}}_A$ is fixed at the preindustrial value of 589 GtC. Also shown are the “lower” and “upper” search bounds of the optimization problem in (7) and (11) for the possible parameter values (see, e.g., Section 2.2 for details on the model parameters and fitting procedure).

solution to physically consistent outcomes.

To justify the selection of the ρ_1 tuning coefficient, we aim to minimize fit error for the time period after $T = 250$, in other word the out-of-sample error with respect μ -benchmark. Figure 3 displays the average absolute error of the emulated atmospheric carbon contented in comparison to the μ -benchmark and dynamic timescales τ , for varying values of ρ_1 . The 3SR model shows minimal sensitivity to the parameter ρ_1 , and the respective q_1 penalty function in (10), which encourages extended dynamic timescales. However, in the 4PR model, we observe improvements in the average absolute errors in most time periods after the initial pulse. As expected, in both model configurations, increasing ρ_1 resulting larger dynamic timescales. The 3SR model can only represent two dynamic timescales, corresponding to two nonzero eigenvalues, whereas the 4PR model can represent three. We observe that the 3SR model, while capable of capturing short-term dynamics, appears to lack the versatility needed to accurately represent short, medium, and long-term timescales simultaneously, tending to average out medium and long-term behaviors. For our tests, we use $\rho_1 = 10^{-2}$ as the selected value for both the 3SR and 4PR configurations.

In the 3SR model configuration, the chosen tuning coefficients are ρ_1 , ρ_2 and ρ_3 , is 10^{-2} , 10^{-4} , and 0.0; while for the 4PR model configuration, the selected values are 10^{-2} , 10^{-4} , and 10^{-4} . With the chosen tuning parameters, the operator \mathbf{A}^μ is defined, and the extremal parameters \mathbf{c}^{μ^+} and \mathbf{c}^{μ^-} can be fitted in accordance with (11). These values are roughly the same for both the 3SR and 4PR model configurations. With the values we can now define the weighted \mathbf{A}^α defined in (12). In Figure A.2, the fitted model is used to depict the emulated decay dynamics of a 100 GtC pulse across different values of α for both model configuration.

The fitted parameters, the parameters search boundaries set for the optimizer, the ratios of oceanic to land-biosphere pulse absorption (denoted as $\mathbf{m}_O^{t_e}/\mathbf{m}_L^{t_e}$) and associated dynamical timescales, are all detailed in Table 1. Notice that, the mass transfer rates \mathbf{a}^μ for the 3SR configuration are notability larger than the 4PR configuration. In contrast, the values of $\tilde{\mathbf{m}}^\mu$ in the 4PR configuration are substantially larger than those in the 3SR configuration and closely align with the equilibrium masses outlined in Ciais et al. (2014) (see the discussion related to (9)). In all tests, the fitted parameters are not non-boundary solutions. The ratios of oceanic to land-biosphere pulse absorption is evaluated at $t_e = 20$, where we expected roughly the ratio to be equal (see, Section 2.2.1 for details), the fitted parameter results in this case we 0.71. While the outcomes of the optimization process³ for tuning coefficients may vary slightly due to factors like the random seed, initial guess, and convergence tolerance, these variations do not substantively affect the overall dynamics of the emulated carbon-cycle. The convergence tolerance for the optimizer is set to 10^{-6} for all tests.

³We emphasize that these values are not necessarily the global optima of the objective function; the optimizer aims to find the global optimum, but achieving this is not guaranteed.

3 Simulations

Understanding the complexities and interconnectedness of climate systems is an imperative for scientific, policy, and societal realms, particularly in the context of accelerating anthropogenic climate change. To this end, computational models that utilize Representative Concentration Pathway (RCP) scenarios provide invaluable insights into future climatic conditions based on a range of potential human activities. While these RCP scenarios—RCP2.6, RCP4.5, RCP6, and RCP8.5—have been widely utilized to study aspects such as temperature rise and precipitation patterns, a comprehensive understanding of atmospheric perturbations and their cascading effects on multi-reservoir systems remains a knowledge gap that demands further exploration.

This section aims to elucidate the novel methodologies and findings of two sets of experiments: Atmospheric Perturbation Tests and Multi-Reservoirs Perturbation Tests. These tests are designed to probe into the intricate dynamics of atmospheric processes and interconnected reservoir systems under varying climate scenarios. Specifically, we apply the RCP scenario datasets for RCP2.6, RCP4.5, RCP6, and RCP8.5 to assess how different levels of radiative forcing impact the stability, resilience, and adaptability of both atmospheric and multi-reservoir systems.

3.1 Atmospheric Perturbation Tests

Lorem ipsum dolor sit amet, consectetur adipiscing elit. Ut purus elit, vestibulum ut, placerat ac, adipiscing vitae, felis. Curabitur dictum gravida mauris. Nam arcu libero, nonummy eget, consectetur id, vulputate a, magna. Donec vehicula augue eu neque. Pellentesque habitant morbi tristique senectus et netus et malesuada fames ac turpis egestas. Mauris ut leo. Cras viverra metus rhoncus sem. Nulla et lectus vestibulum urna fringilla ultrices. Phasellus eu tellus sit amet tortor gravida placerat.

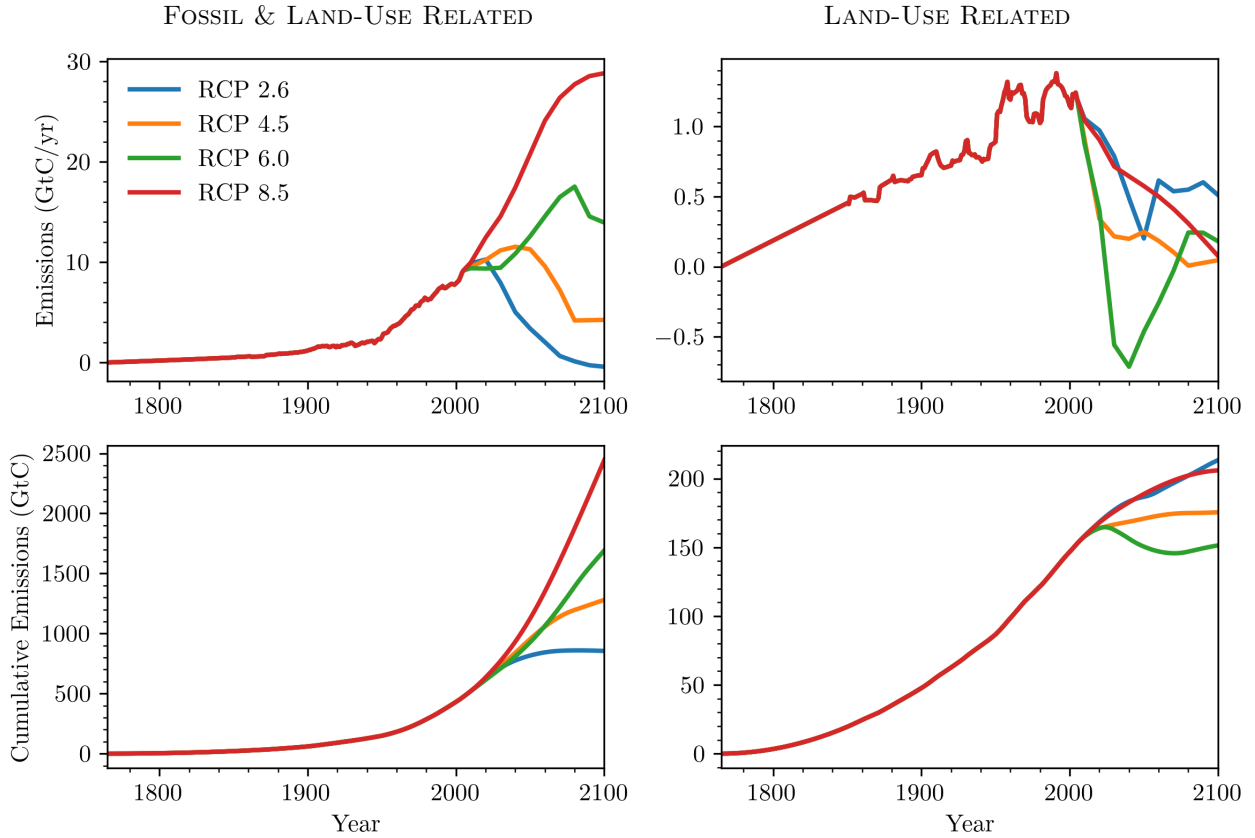


Figure 4: Emissions total and land, incmrneatla an cumsum .

3.1.1 Pulse

Lorem ipsum dolor sit amet, consectetur adipiscing elit. Ut purus elit, vestibulum ut, placerat ac, adipiscing vitae, felis. Curabitur dictum gravida mauris. Nam arcu libero, nonummy eget, consectetur id, vulputate a, magna. Donec vehicula augue eu neque. Pellentesque habitant morbi tristique senectus et netus et malesuada fames ac turpis egestas. Mauris ut leo. Cras viverra metus rhoncus sem. Nulla et lectus vestibulum urna fringilla ultrices. Phasellus eu tellus sit amet tortor gravida placerat. Integer sapien est, iaculis in, pretium quis, viverra ac, nunc. Praesent eget sem vel leo ultrices bibendum. Aenean faucibus. Morbi dolor nulla, malesuada eu, pulvinar at, mollis ac, nulla. Curabitur auctor semper nulla. Donec varius orci eget risus. Duis nibh mi, congue eu, accumsan eleifend, sagittis quis, diam. Duis eget orci sit amet orci dignissim rutrum. Lorem ipsum dolor sit amet, consectetur adipiscing elit. Ut purus elit, vestibulum ut, placerat ac, adipiscing vitae, felis. Curabitur dictum gravida mauris. Nam arcu libero, nonummy eget, consectetur id, vulputate a, magna. Donec vehicula augue eu neque. Pellentesque habitant morbi tristique senectus et netus et malesuada fames ac turpis egestas. Mauris ut leo. Cras viverra metus rhoncus sem. Nulla et lectus vestibulum urna fringilla ultrices. Phasellus eu tellus sit amet tortor gravida placerat. Integer sapien est, iaculis in, pretium quis, viverra ac, nunc. Praesent eget sem vel leo ultrices bibendum. Aenean faucibus. Morbi dolor nulla, malesuada eu, pulvinar at, mollis ac, nulla. Curabitur auctor semper nulla. Donec varius orci eget risus. Duis nibh mi, congue eu, accumsan eleifend, sagittis quis, diam. Duis eget orci sit amet orci dignissim rutrum.

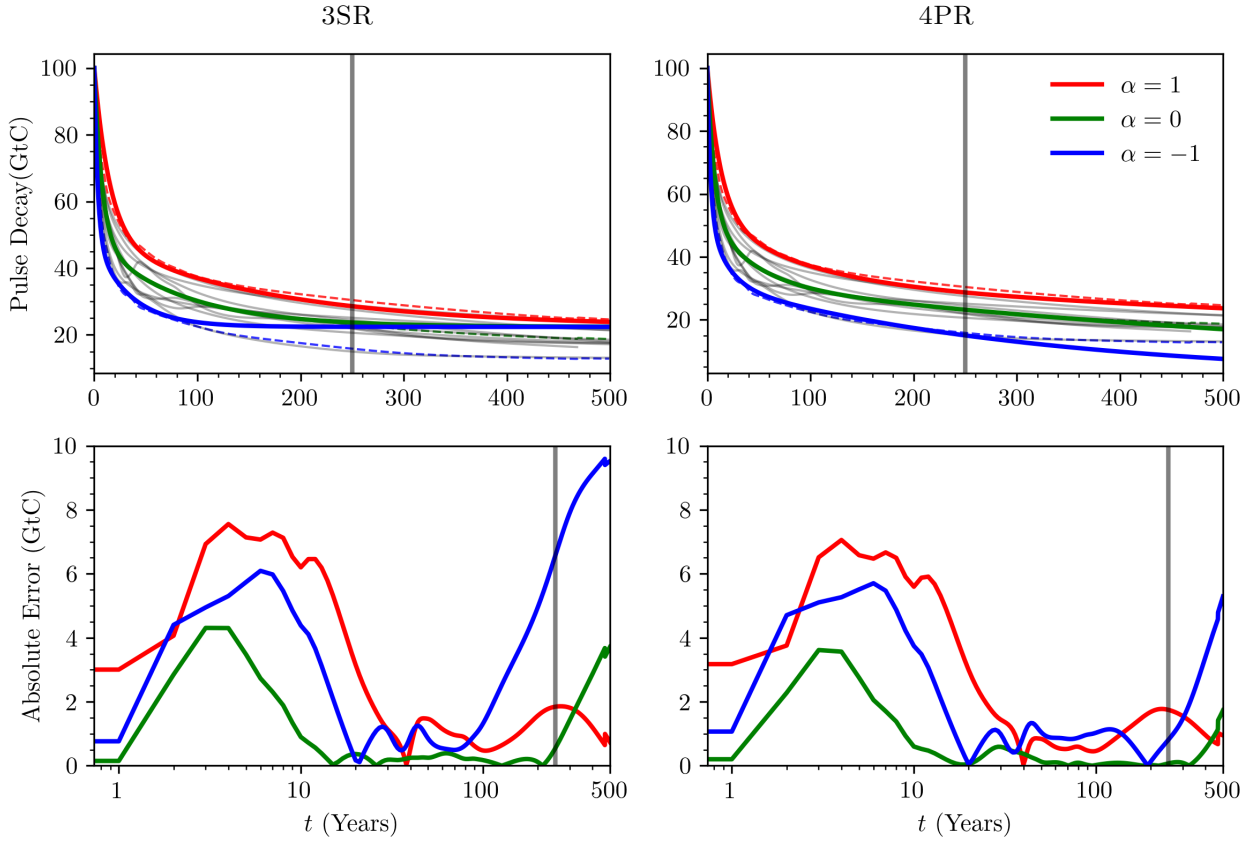


Figure 5: Lorem ipsum dolor sit amet, consectetur adipiscing elit. Ut purus elit, vestibulum ut, placerat ac, adipiscing vitae, felis. Curabitur dictum gravida mauris. Nam arcu libero, nonummy eget, consectetur id, vulputate a, magna. Donec vehicula augue eu neque.

3.1.2 macdougall

This test represents the protocol for the Zero Emissions Commitment Model Intercomparison Project (ZECMIP) is designed to examine how carbon emissions and subsequent zero-emissions states affect climate variables over time. Here we will outline what is referred to as Type A tests, in which the simulations begin at pre-industrial (PI) conditions. In these tests, we create emissions resulting in a 1% increase in atmospheric carbon content, until the total emission reaches 1000 GtC. Once the target cumulative emission is reached, models switch to a mode where no further CO₂ emissions are introduced, allowing for the free evolution of the model. Given that no more anthropogenic CO₂ is being emitted, the atmospheric CO₂ concentration is expected to decline due to natural carbon uptake by the ocean and land. Each model operator \mathbf{A}^α or each model configuration in the simulation is initialized in different years depending on when the model reaches the target cumulative emissions, influenced by the model's representation of carbon cycle feedbacks. Each model operator \mathbf{A}^α or each model configuration in the simulation is initialized in different years depending on when the model reaches the target cumulative emissions, influenced by the model's representation of carbon cycle feedbacks. Each model operator \mathbf{A}^α or each model configuration in the simulation is initialized in different years depending on when the model reaches the target cumulative emissions, influenced by the model's representation of carbon cycle feedbacks. Each model operator \mathbf{A}^α or each model configuration in the simulation is initialized in different years depending on when the model reaches the target cumulative emissions, influenced by the model's representation of carbon cycle feedbacks.

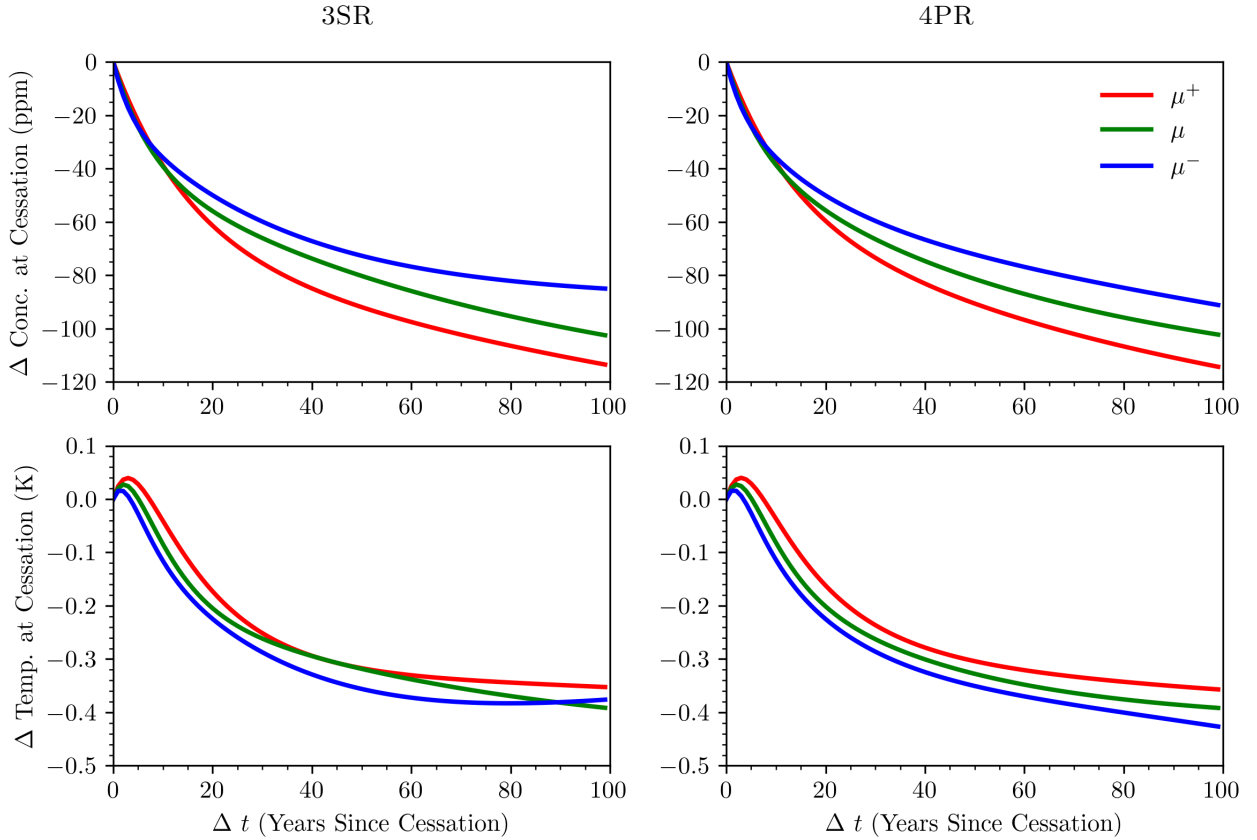
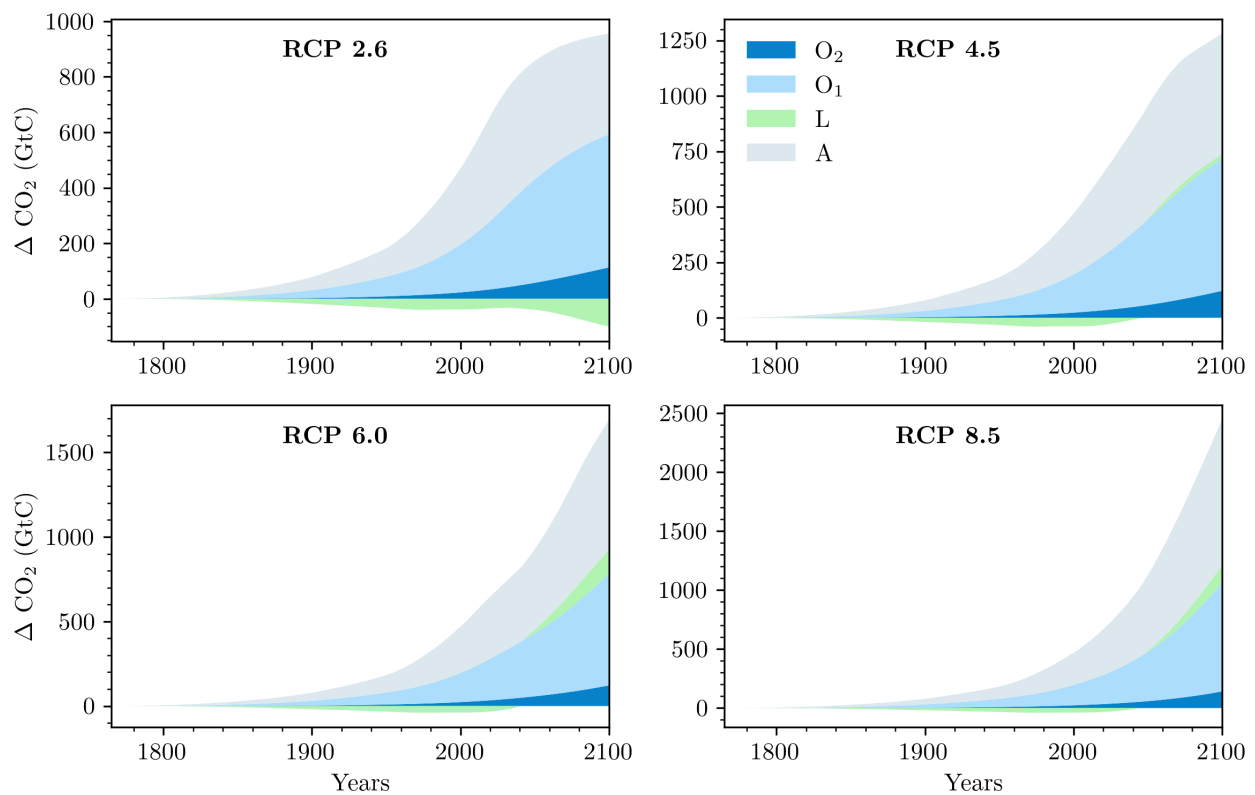


Figure 6: Each model operator \mathbf{A}^α or each model configuration in the simulation is initialized in different years depending on when the model reaches the target cumulative emissions, influenced by the model's representation of carbon cycle feedbacks.

3.2 Representative Concentration Pathway

metus rhoncus sem. Nulla et lectus vestibulum urna fringilla ultrices. Phasellus eu tellus sit amet tortor gravida placerat. Integer sapien est, iaculis in, pretium quis, viverra ac, nunc. Praesent eget sem vel leo ultrices bibendum. Aenean faucibus. Morbi dolor nulla, malesuada eu, pulvinar at, mollis ac, nulla. Curabitur auctor semper nulla. Donec varius orci eget risus. Duis nibh mi, congue eu, accumsan eleifend, sagittis quis, diam. Duis eget orci sit amet orci dignissim rutrum. Lorem ipsum dolor sit amet, consectetur adipiscing elit. Ut purus elit, vestibulum ut, placerat ac, adipiscing vitae, felis. Curabitur dictum gravida mauris. Nam arcu libero, nonummy eget, consectetur id, vulputate a, magna. Donec vehicula augue eu neque. Pellentesque habitant morbi tristique senectus et netus et malesuada fames ac turpis egestas. Mauris ut leo. Cras viverra metus rhoncus sem. Nulla et lectus vestibulum urna fringilla ultrices. Phasellus eu tellus sit amet tortor gravida placerat. Integer sapien est, iaculis in, pretium quis, viverra ac, nunc. Praesent eget sem vel leo ultrices bibendum. Aenean faucibus. Morbi dolor nulla, malesuada eu, pulvinar at, mollis ac, nulla. Curabitur auctor semper nulla. Donec varius orci eget risus. Duis nibh mi, congue eu, accumsan eleifend, sagittis quis, diam. Duis eget orci sit amet orci dignissim rutrum.



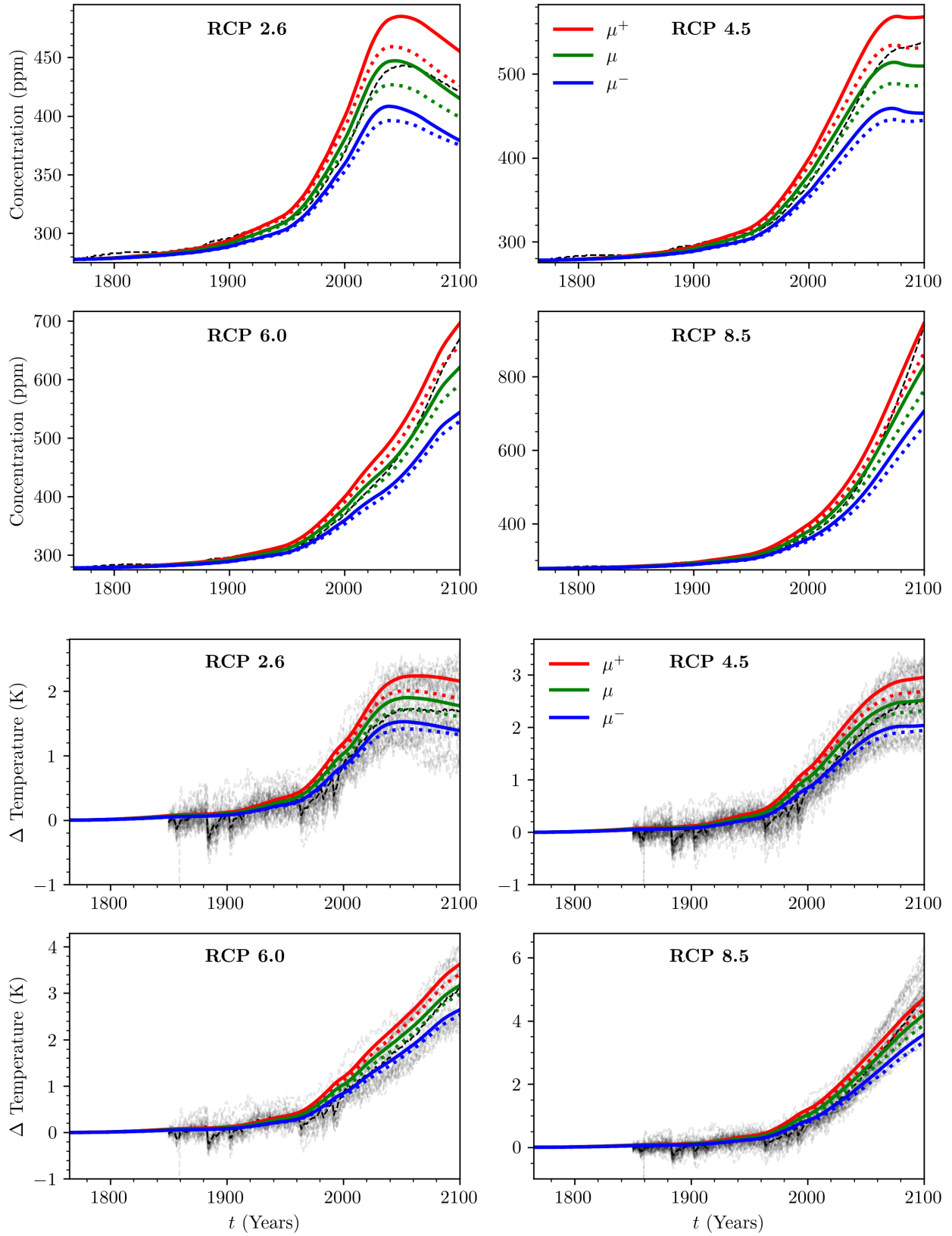


Figure 9: 3SR (dotted line) 4PR (solid lines). The 4PR simulation augments the land-biosphere equilibrium masses based on land-use related emission in Figure 4. 4PR captures both the co₂ and temp better than 3sr.

A Climate Emulator

PENALTY FUNCTIONS AND EMULATOR CHARACTERISTICS

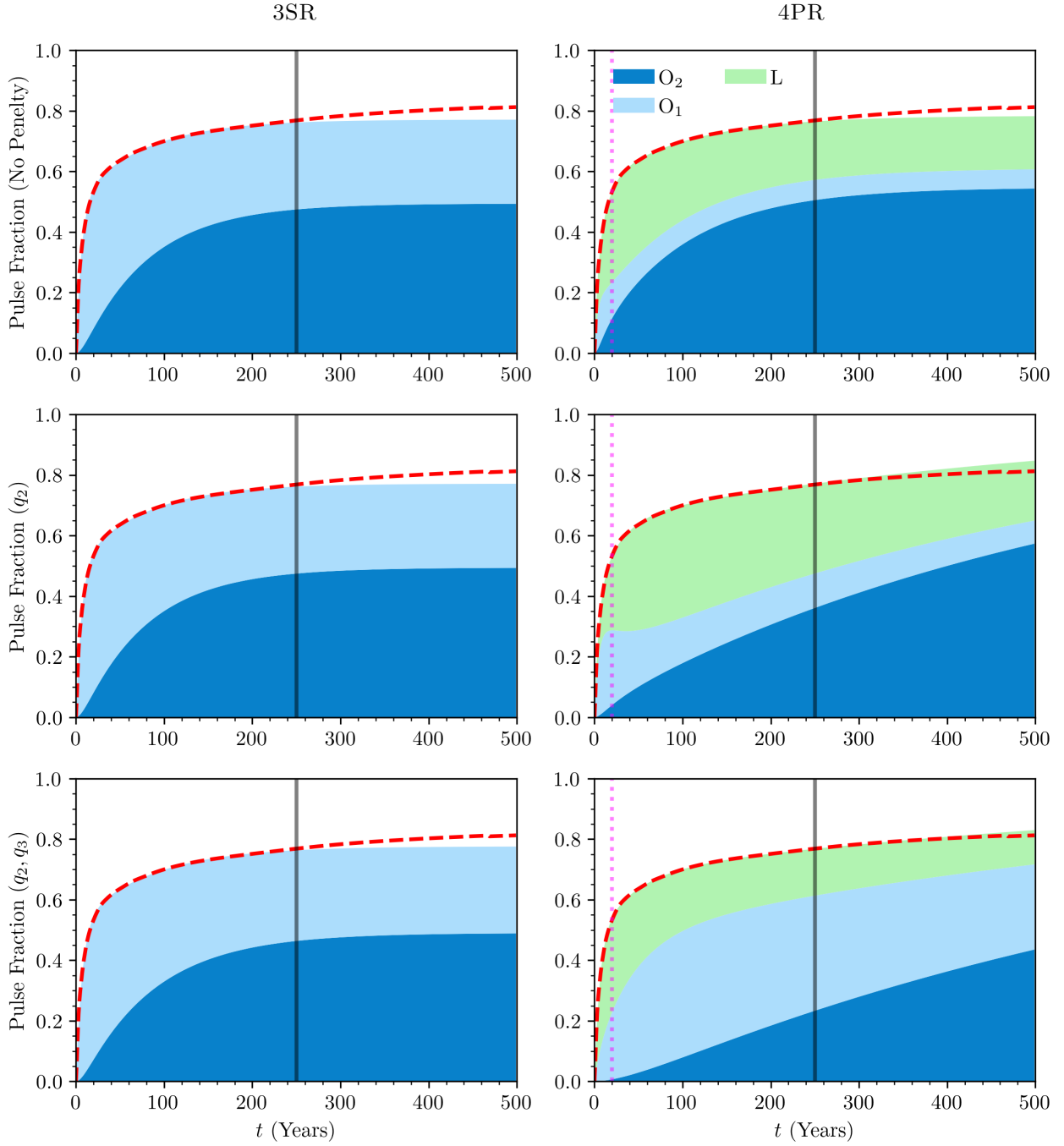


Figure A.1: A visualization of the fraction of a 100 GtC pulse of emissions absorbed by different reservoirs in the 3SR (left column) and 4PR (right column) model configurations over 500 years. This data is based on a series of controlled simulations conducted by Joos et al. (2013). For further details on the simulations and model descriptions, we refer the reader to the cited reference. The multimodal mean of the simulations, denoted by μ , along with the two standard deviations above and below μ -benchmark, are represented by μ^+ and μ^- , respectively.

PRE-INDUSTRIAL PULSE DECAY

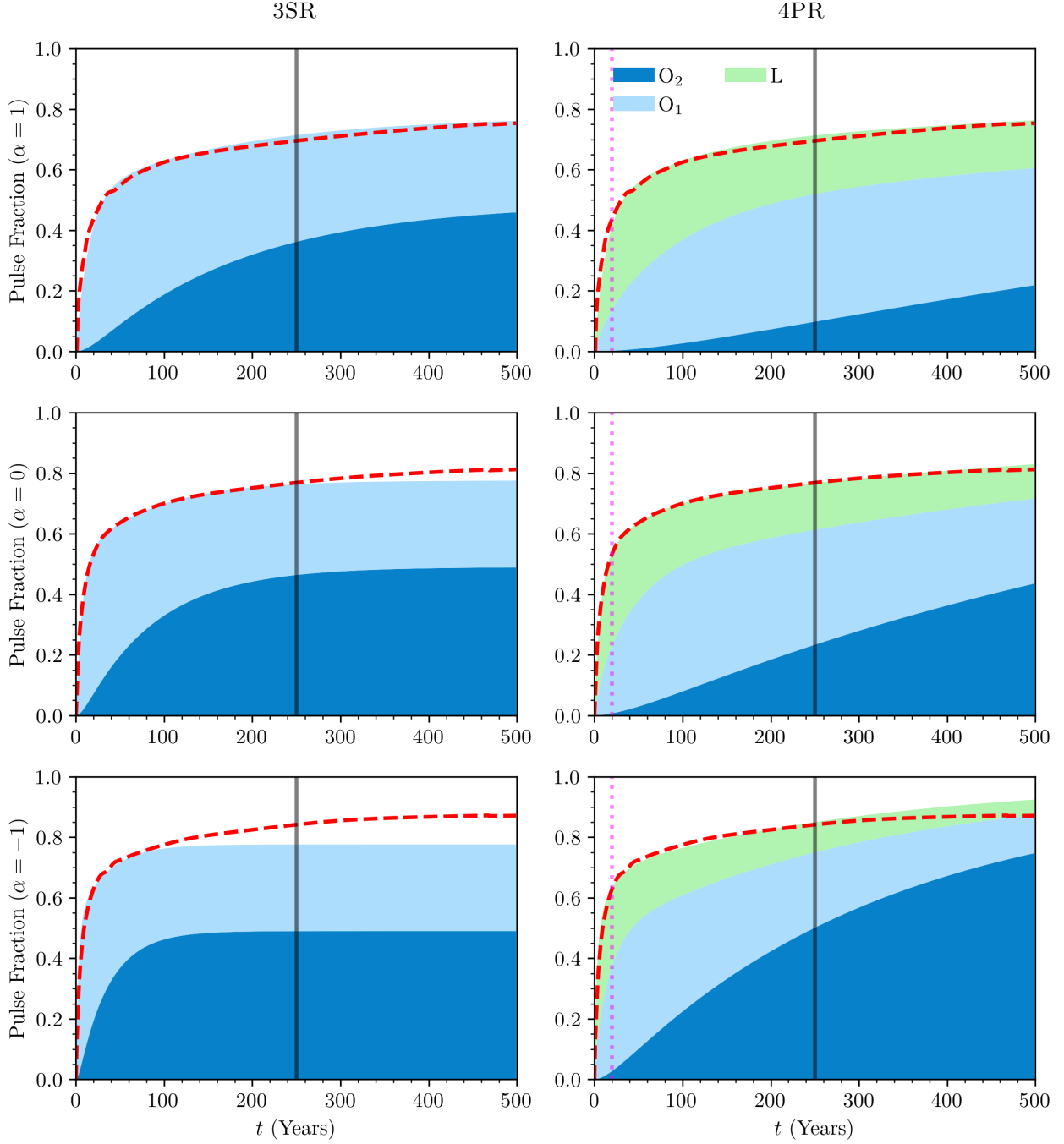


Figure A.2: A visualization of the fraction of a 100 GtC pulse of emissions absorbed by different reservoirs in the 3SR (left column) and 4PR (right column) model configurations over 500 years. For each model configuration, we display the model dynamics using α equal to 1, 0, and -1 , corresponding to different calibrations of the model parameter representing slow, average, and fast rates of carbon absorption from the atmosphere, respectively. Model calibration and fitted parameters are outlined in Table 1, based on the procedure described in Section 2.2. In the pulse scenario, the experiment is based on pre-industrial conditions from 1765, with a dashed red line serving as the benchmark simulation derived from various Earth System Models (ESMs) of differing complexities (for further details, see Joos et al. (2013)). The benchmark simulation for $\alpha = 0$ represents the mean of the different ESMs, while $\alpha = 1$ and $\alpha = -1$ correspond to two standard deviations above and below the mean, respectively. The vertical solid black line at $t = 250$ represents the time up to which the model calibration is performed, denoted as $T = t$ in (6). The simulation for $t \leq T$ are considered in-sample results, while those for $t > T$ are out-of-sample. The vertical dotted purple line at $t = 20$ indicates an expected one-to-one carbon absorption ratio between the ocean and land-biosphere (see Section 2.2.1).

ZERO EMISSIONS COMMITMENT MODEL INTERCOMPARISON PROJECT (ZECMIP)—EXPERIMENT
TYPE A

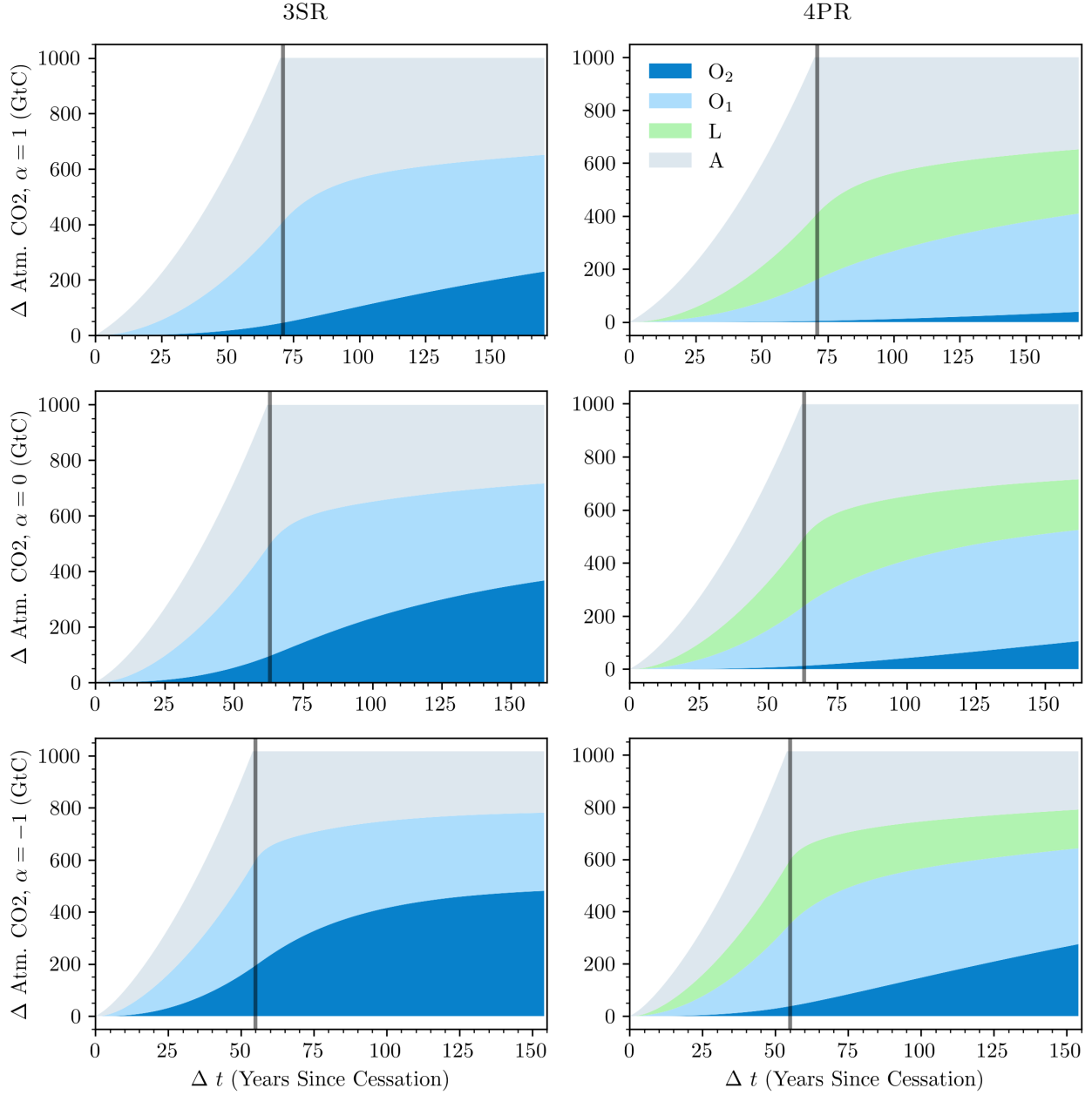


Figure A.3: Each model operator \mathbf{A}^α or each model configuration in the simulation is initialized in different years depending on when the model reaches the target cumulative emissions, influenced by the model's representation of carbon cycle feedbacks. Each model operator \mathbf{A}^α or each model configuration in the simulation is initialized in different years depending on when the model reaches the target cumulative emissions, influenced by the model's representation of carbon cycle feedbacks.

BASELINE CO₂ CONCENTRATION AND TEMPERATURE FOR RCP SCENARIOS

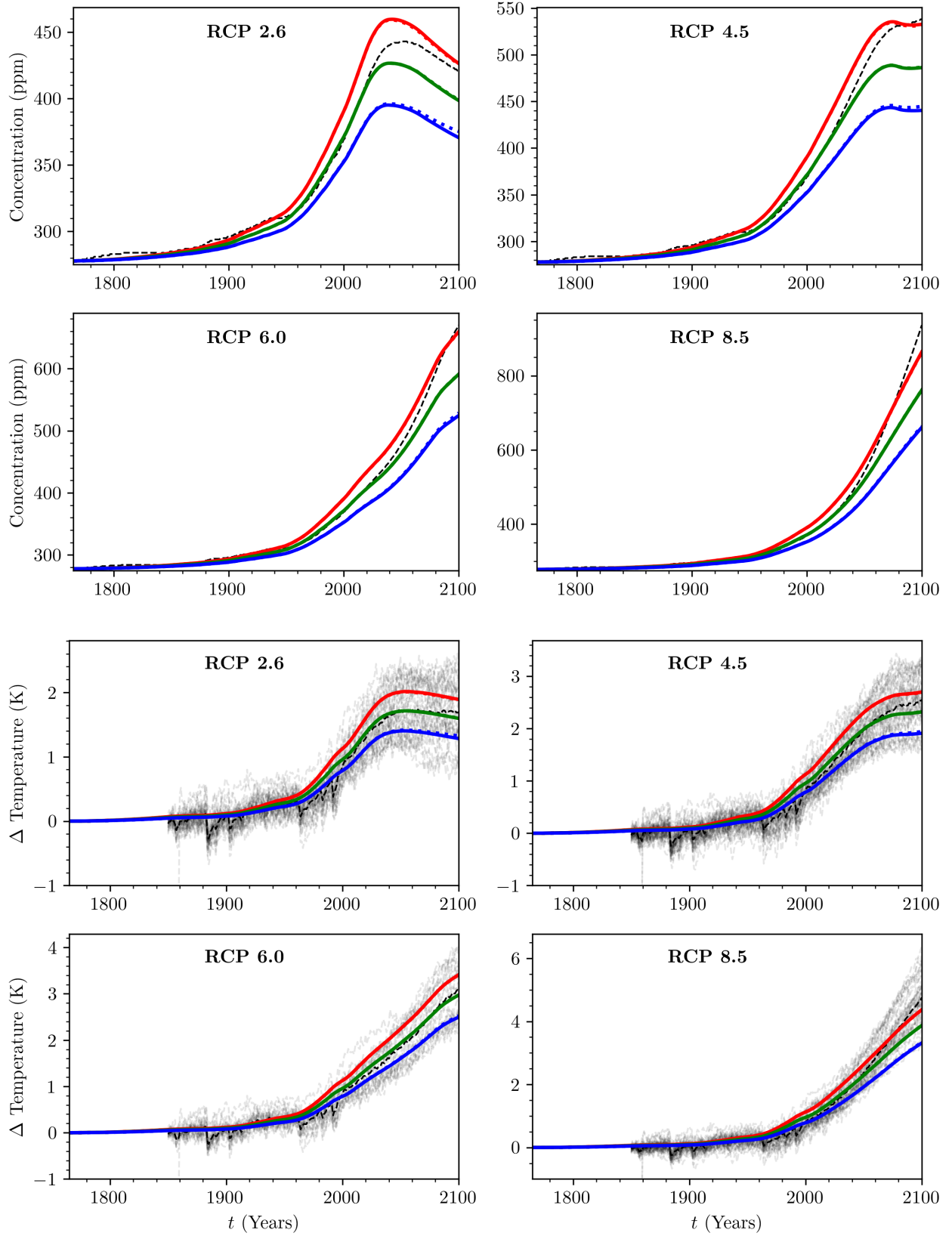
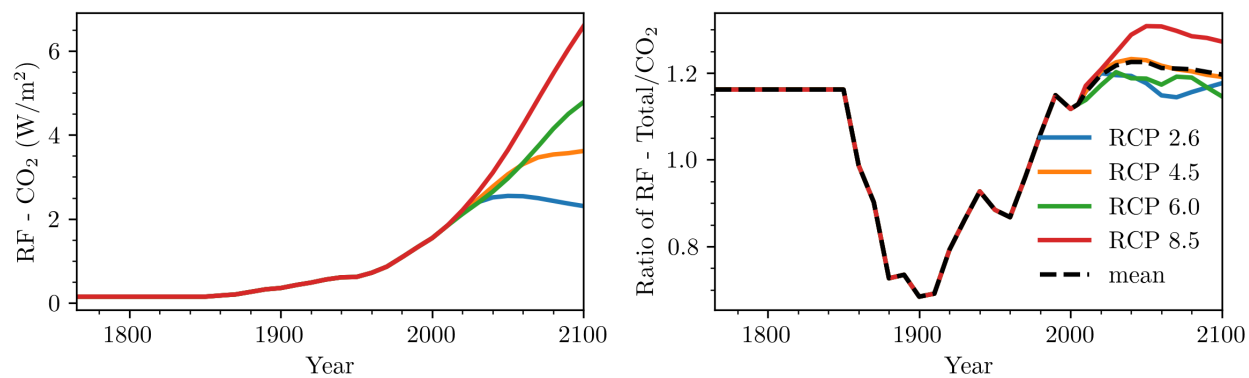


Figure A.4: 3SR (dotted line) 4PR (solid lines). Here the 4PR simulation DOES NOT augment the land-biosphere equilibrium masses based on land-use related emission in Figure 4. 4PR behaves almost identical to 3SR model.

B Temperature Model

Decsription of two layer temperature modele described in matrix form .

[illegible]

Bibliographies

- Ciais, P., C. Sabine, G. Bala, L. Bopp, V. Brovkin, et al., and Joanna Isobel House. 2014. Carbon and Other Biogeochemical Cycles. United Kingdom: Cambridge University Press, 465–570.
- Joos, Fortunat, Raphael Roth, Jan S Fuglestad, Glen P Peters, Ian G Enting, W von Bloh, Victor Brovkin, Eleanor J Burke, Michael Eby, Neil R Edwards et al. 2013. “Carbon dioxide and climate impulse response functions for the computation of greenhouse gas metrics: a multi-model analysis.” Atmospheric Chemistry and Physics 13 (5):2793–2825.